

Magnetic Signature of Chiral Phonons Revealed by Neutron Spectroscopy in Ferrimagnetic $\text{Fe}_{1.75}\text{Zn}_{0.25}\text{Mo}_3\text{O}_8$

Song Bao,^{1,2,*} Junbo Liao,^{1,†} Zhentao Huang,^{1,3,4,†} Yanyan Shangguan,¹ Zhen Ma,⁵ Bo Zhang,¹ Shufan Cheng,¹ Hao Xu,¹ Zihang Song,¹ Shuai Dong,¹ Maofeng Wu,¹ Ryoichi Kajimoto,⁶ Mitsutaka Nakamura,⁶ Tom Fennell,⁷ Dmitry Khalyavin,⁸ and Jinsheng Wen^{1,2,‡}

¹*National Laboratory of Solid State Microstructures and Department of Physics, Nanjing University, Nanjing 210093, China*

²*Collaborative Innovation Center of Advanced Microstructures and Jiangsu Physical Science Research Center, Nanjing University, Nanjing 210093, China*

³*Institute of High Energy Physics, Chinese Academy of Sciences (CAS), Beijing 100049, China*

⁴*Spallation Neutron Source Science Center, Dongguan 523803, China*

⁵*Hubei Key Laboratory of Photoelectric Materials and Devices, School of Materials Science and Engineering, Hubei Normal University, Huangshi 435002, China*

⁶*J-PARC Center, Japan Atomic Energy Agency (JAEA), Tokai, Ibaraki 319-1195, Japan*

⁷*PSI Center for Neutron and Muon Sciences, Paul Scherrer Institut, 5232 Villigen PSI, Switzerland*

⁸*ISIS Facility, STFC Rutherford Appleton Laboratory, Chilton, Didcot, Oxfordshire OX11 0QX, United Kingdom*

Lattice vibrations can carry angular momentum and magnetic moments under broken inversion or time-reversal symmetry, forming so-called chiral phonons. While such excitations have been explored in nonmagnetic systems via optical probes, their direct detection in magnetic materials and coupling to spin excitations remain largely unexplored. Here, using neutron spectroscopy, sensitive to both nuclear and magnetic scattering, we reveal the magnetic signature of chiral phonons in ferrimagnetic $\text{Fe}_{1.75}\text{Zn}_{0.25}\text{Mo}_3\text{O}_8$ with Curie temperature $T_C \sim 49$ K. Below T_C , we observe enhanced magnetic scattering of phonons at small momenta, arising from strong magnon-phonon coupling. In addition, out-of-plane intensity modulation, phonon mode splitting, and field-induced Zeeman shifts are observed, all closely associated with the ferrimagnetic order. These features vanish above T_C , where phonon spectra are dominated by nuclear scattering. These observations demonstrate the existence of chiral phonons carrying substantial magnetic moments that directly contribute to magnetic scattering, and establish neutron spectroscopy as a powerful, momentum-resolved probe of their magnetic character.

Chiral phonons are collective vibrational modes in crystals, characterized by circularly polarized ionic motions carrying nonzero angular momentum. They were initially proposed and observed in two-dimensional systems with broken inversion symmetry^{1–4}, where the rotational mode propagates within the plane of rotation. Subsequent studies extended these ideas to three-dimensional chiral crystals, including α -HgS⁵, quartz⁶ and Te⁷, where chiral phonons were demonstrated to exhibit nonzero helicity^{8,9}, with their angular momentum having a finite projection along the phonon propagation direction—a feature absent in their two-dimensional counterparts. The chirality and angular momentum of phonons have emerged as fundamental concepts in lattice dynamics, giving rise to a variety of exotic phenomena, including Einstein-de Haas effect^{1,10,11}, phonon magnetism^{12–15}, phonon Zeeman effect^{16–18}, and phonon Hall effect^{19–22}. More recently, increasing attention has focused on the interplay between chiral phonons and other degrees of freedom, including charge, spin, orbital, and topology^{23–37}, opening new avenues for manipulating phonon-driven phenomena in complex quantum materials.

Despite these advances, most existing studies have focused on nonmagnetic systems^{1–9,23–25,29–31}, leaving the coupling between chiral phonons and magnetic

order, particularly their interactions with magnons, largely unexplored^{26,27,32–37}. Experimentally, investigations have so far relied primarily on optical techniques, such as Raman scattering^{5,7,32,35,36}, infrared and terahertz spectroscopy^{4,29–31}, and resonant inelastic X-ray scattering^{6,38}. These methods utilize the (pseudo-)angular momentum transfer between circularly polarized photons and chiral phonons^{2,5,7,9}, but are inherently limited in their ability to map the full energy-momentum dispersions of chiral phonons.

In contrast, neutron scattering offers a powerful alternative by providing simultaneous access to both nuclear and magnetic scattering cross sections of chiral phonons, thereby enabling momentum-resolved studies. As illustrated in Fig. 1(a), in conventional linear phonon scattering processes, the signal arises predominantly from nuclear scattering, reflecting the displacement of atomic nuclei. In principle, neutrons can also probe the magnetic response associated with phonon excitations, which in the context of chiral phonons originates from their intrinsic phonon magnetic moments—a consequence of the circular motion of charged ions. These moments are typically on the order of the nuclear magneton (μ_N)^{16–18}, far smaller than electronic spin or orbital moments measured in Bohr magnetons (μ_B), and thus usually produce negligible magnetic scattering. However, in

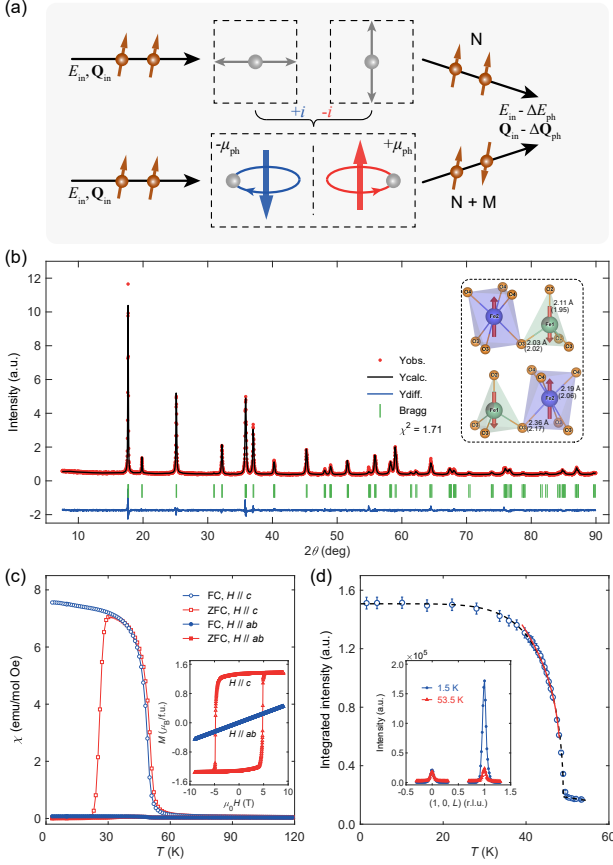


FIG. 1. (a) Schematic of neutron probing of lattice vibrations: conventional linear phonons give only nuclear (N) scattering, whereas chiral phonons with phonon magnetic moments (μ_{ph}) yield both N and magnetic (M) signals. (b) Room-temperature powder XRD pattern and Rietveld refinement. Inset: ferrimagnetic structure and Zn-induced lattice distortions in FZMO, with Fe-O bond lengths labeled (values for FMO in parentheses). (c) Magnetic susceptibility of an FZMO single crystal under zero-field-cooled (ZFC) and field-cooled (FC) conditions in a 0.1-T field. Inset: M - H curves at 10 K. (d) Temperature dependence of the integrated intensity of the $(1, 0, 1)$ magnetic Bragg peak measured on EIGER. Error bars denote one standard deviation throughout the paper. The red curve is a power-law fit and the dashed line is a guide to the eye. Inset: elastic scans along $(1, 0, L)$ at 1.5 and 53.5 K.

systems with strong electron-, orbital-, or spin-phonon coupling^{29–35}, the effective magnetic moment of chiral phonons can be significantly enhanced, reaching the μ_B scale. Under such conditions, magnetic scattering from chiral phonons becomes appreciable, opening a pathway for momentum-resolved investigations of chiral phonons and their coupling to various static orders and collective excitations^{23–37}.

$\text{Fe}_{2-x}\text{Zn}_x\text{Mo}_3\text{O}_8$ is a type-I multiferroic system exhibiting colossal linear magnetoelectricity and a giant thermal Hall effect^{39–42}, indicative of strong spin-lattice coupling. In previous studies of the parent compound

$\text{Fe}_2\text{Mo}_3\text{O}_8$ (FMO), we observed topological magnon polarons arising from strong magnon-phonon coupling³⁴ and a pair of degenerate chiral phonon modes carrying substantial magnetic moments, up to $0.68 \mu_B$ ³⁵. The magnetic configuration of FMO can also be tuned by external fields or chemical doping, inducing a metamagnetic transition from an antiferromagnetic to a ferrimagnetic state^{39,40}. These properties establish FMO and its derivatives as an ideal platform to study how magnetic-order symmetry influences chiral phonons under strong magnon-phonon coupling, while the sizable phonon magnetic moments facilitate direct, momentum-resolved detection by neutron scattering.

In this work, we perform inelastic neutron scattering (INS) to investigate the excitation spectra of 12.5% Zn-doped $\text{Fe}_{1.75}\text{Zn}_{0.25}\text{Mo}_3\text{O}_8$ (FZMO), which hosts a collinear ferrimagnetic ground state below $T_C \sim 49$ K. At 6 K, the excitation spectra reveal three intense magnon branches, along with signatures of hybridization and gap openings between magnon and phonon bands, indicative of strong magnon-phonon coupling. Low-energy phonons generate measurable magnetic scattering, particularly at small momenta. These modes exhibit out-of-plane intensity modulation, pronounced splitting, and field-induced Zeeman shifts, all closely linked to the underlying ferrimagnetic order. These features vanish above T_C . Our results provide a rare momentum-resolved mapping of chiral phonons and their magnetic signatures in magnetic systems.

Single crystals of FZMO were grown using chemical vapor transport method (see Note 1 in Supplemental Material (SM) for details⁴³). Powder X-ray diffraction (XRD) shows that Zn preferentially occupies the tetrahedral Fe1 sites while retaining the polar $P6_3mc$ symmetry, consistent with earlier studies^{39,55,56}. Rietveld refinements indicate that Zn substitution primarily perturbs the coordinating oxygen positions and induces local lattice distortions, particularly around the octahedral Fe2 environment (inset of Fig. 1(b) and Note 2 in SM⁴³), likely modifying the crystal field and single-ion anisotropy. Magnetic susceptibility measurements reveal ferrimagnetic ordering below $T_C \sim 49$ K with strong easy-axis anisotropy, in agreement with elastic neutron results [Figs. 1(c) and 1(d)]. This ferrimagnetic state results from selective dilution of the Fe1 sublattice, altering the balance of interlayer couplings (Note 3 in SM⁴³). A power-law fit yields a critical exponent $\beta = 0.170$, slightly above the 2D Ising value observed in FMO^{34,58}.

Figures 2(a)-2(c) show the overall excitation spectra of FZMO measured along high-symmetry directions [Figs. 2(d) and 2(e)]. Guided by our previous study on FMO³⁴, we identify three types of excitations within the same energy-momentum window: (i) three intense, weakly dispersive magnon branches at higher energies (10–20 meV); (ii) several weak, strongly dispersive phonon modes originating from low energies; and (iii) magnon-phonon hybrid excitations—magnon-polarons—emerging near the intersections between the magnon and

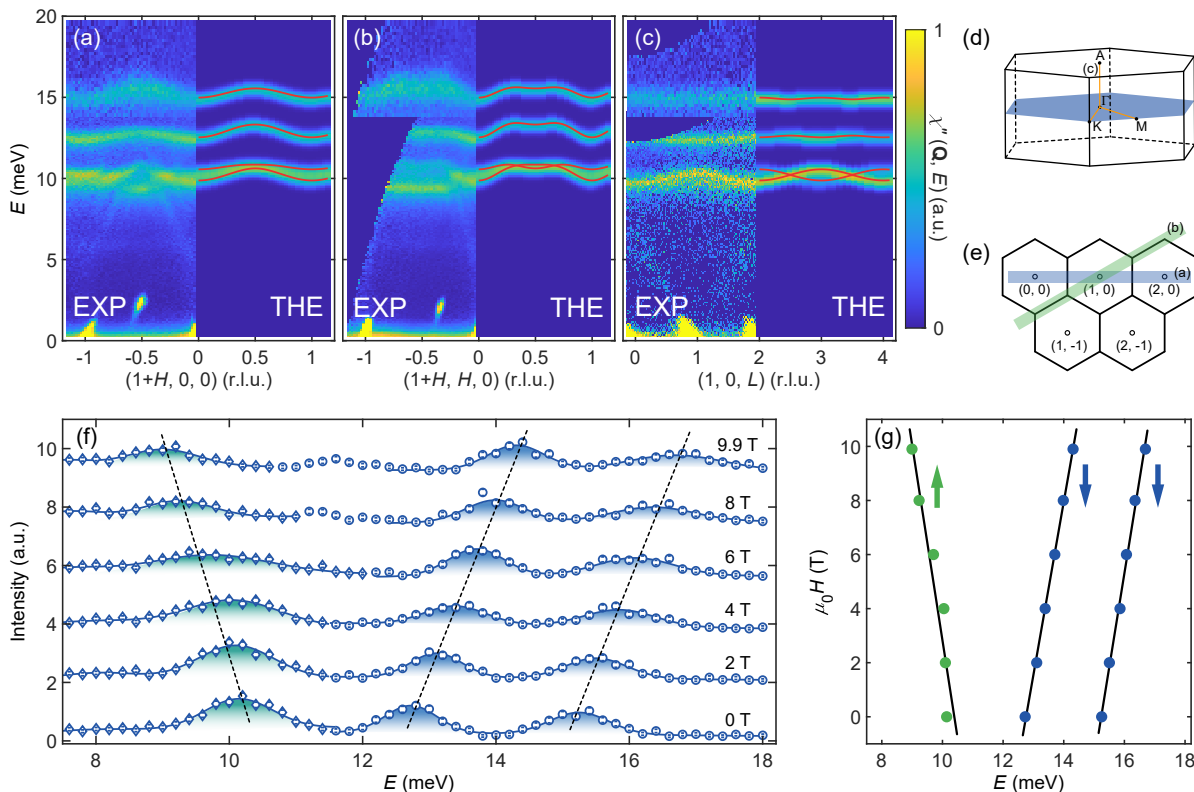


FIG. 2. (a)-(c) INS spectra of FZMO at 6 K along the [100], [110], and [001] (left), compared with calculated spin-wave spectra (right). Data were measured on 4SEASONS with $E_i = 18$ and 30 meV, scaled to incoherent elastic scattering. Integration ranges are listed in Table S3⁴³. (d), (e) Brillouin zone in 3D and its 2D projection with high-symmetry paths. (f) Energy scans at $(1.2, 0, 0)$ under varying magnetic fields, measured on EIGER. Diamonds and circles denote data collected in normal- and high-resolution configurations, respectively, with vertical offsets applied for clarity. Curves are Gaussian fits and dashed lines are guides to the eye. (g) Extracted peak positions as a function of field, compared with model predictions (solid lines). Up and down arrows denote spin quantum numbers $\Delta S_z = +1$ and -1 .

phonon bands.

Notably, the three intense magnon branches exceed the two nearly doubly-degenerate branches expected from linear spin-wave theory for a bipartite ferrimagnet⁵⁷. This anomaly is captured by a minimal spin model incorporating site-dependent anisotropy and interlayer coupling (Note 3 in SM⁴³). The model yields two nearly degenerate Fe1-derived modes with $\Delta S_z = +1$, and two separate Fe2-derived modes with $\Delta S_z = -1$. The latter separation is attributed to Zn-substitution-induced local distortions, which creates two distinct Fe2 environments with different single-ion anisotropies, consistent with structural considerations and prior reports of stronger anisotropy at Fe2 sites in the parent compound (Notes 2 and 3 in SM⁴³). The field evolution further supports this assignment: the lowest branch softens while the two higher branches harden with increasing field [Figs. 2(f) and 2(g)], consistent with their opposite ΔS_z signs.

Having identified the distinct excitation types, we now examine the low-energy phonon spectra to understand how strong magnon-phonon coupling shapes the lattice dynamics in the ferrimagnetic state. At 6 K,

phonon excitations are visible across both small and large momenta [Figs. 3(a)-3(c)]. In contrast, at 100 K, their intensity is strongly suppressed at small momenta [Figs. 3(d) and 3(e)], but remains visible at larger momenta [Fig. 3(f)]. The enhanced spectral weight at small momenta at 6 K arises from additional magnetic scattering due to off-resonant magnon-phonon coupling, whose magnitude depends on the coupling strength, the detuning between the two excitations, and the magnon magnetic moment^{35,59}. This magnetic contribution is superimposed on the nuclear phonon signal. At 100 K, it disappears as the ferrimagnetic order vanishes, and the phonon intensities follow the expected momentum dependence of purely nuclear scattering, becoming more prominent at larger momenta.

A detailed examination of the phonon spectra reveals a saddle point near 5.5 meV, featuring a minimum along [100] and a maximum along [001] shown in Figs. 3(a)-3(c). Our previous studies have shown that such zone-center excitations correspond to a pair of degenerate chiral phonons that carry substantial phonon magnetic moments in antiferromagnetic FMO^{34,35}. In ferrimagnetic FZMO, similar excitations persist but exhibit a distinct

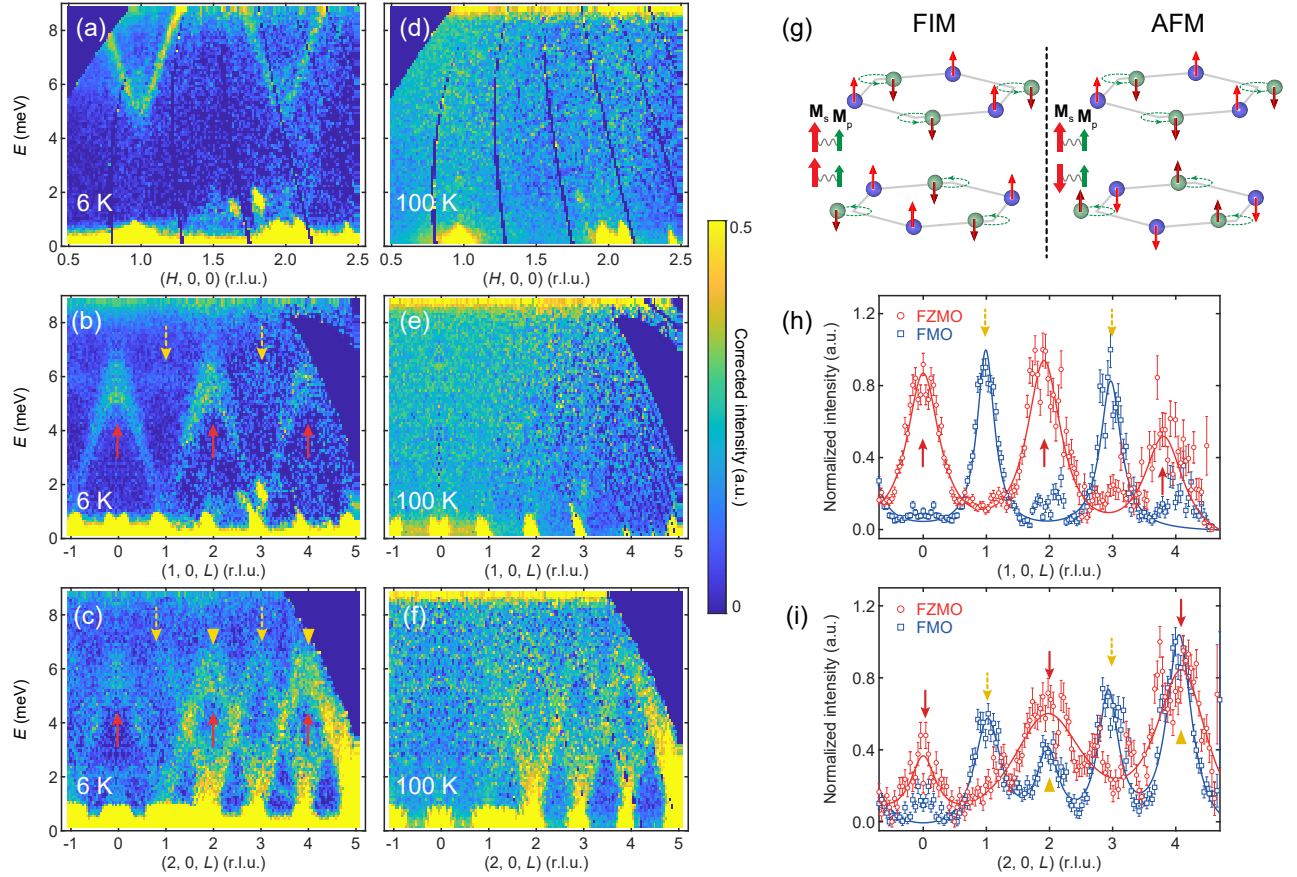


FIG. 3. (a)-(c) Phonon spectra at 6 K along $(H, 0, 0)$, $(1, 0, L)$, and $(2, 0, L)$. (d)-(f) Corresponding spectra at 100 K. Data with $E_i = 12$ meV are corrected by Bose factor. (g) Schematic illustrating the coupling between phonon magnetic moments (M_p) arising from in-plane rotation of Fe1 ions (right-handed example shown) and net spin moments (M_s) in adjacent layers for ferrimagnetic (FIM) and antiferromagnetic (AFM) states. (h) Constant- E cuts along $(1, 0, L)$ for FZMO (red circles) and FMO (blue squares). (i) Corresponding cuts along $(2, 0, L)$. The energy interval is 5.4 ± 0.4 meV. Curves are Lorentzian fits. Solid (dashed) arrows mark intense zone-center chiral optical phonons in FZMO (FMO), while triangles indicate dominant nuclear scattering contributions in (h), (i); the same symbols appear in (b), (c) for guidance.

out-of-plane intensity modulation. Specifically, enhanced phonon intensity appears at even L , marked by solid arrows in Figs. 3(b) and 3(c), whereas FMO shows odd- L modulation, indicated by dashed arrows. A detailed comparison is provided by constant- E cuts across the saddle points in Figs. 3(h) and 3(i). Exceptions occur at large momenta such as $(2, 0, 2)$ and $(2, 0, 4)$, where strong nuclear scattering dominates, as also observed at 100 K [Fig. 3(f)]. It is worth noting that the 12.5% Zn substitution in FZMO does not alter the parent polar structure [Fig. 1(b)], and the nuclear dynamic structure factor alone cannot account for the reversed intensity modulation. This is confirmed by measurements at 100 K, where FZMO and FMO exhibit nearly identical phonon spectra without any L -dependent modulation [Figs. 3(d)-3(f); Ref. 34]. Instead, the reversal emerges only below the magnetic ordering temperatures, indicating its close connection to the underlying magnetic configurations. A plausible explanation is that the phonon modes acquire a magnetic component, i.e., chiral phonons carrying an-

gular momenta and effective magnetic moments, which couple to the spin order, as illustrated in Fig. 3(g). The distinct coupling forms, arising from the relative orientations of phonon magnetic moments and net spin moments in adjacent layers, lead to constructive interference at even L and extinction at odd L in the ferromagnetic stacking of FZMO, whereas the opposite pattern appears in the antiferromagnetic stacking of FMO. A detailed analysis is provided in Note 4 of the SM⁴³.

In addition to the spectral weight modulation, the ferrimagnetic order also induces an intrinsic splitting of the chiral phonons. As shown in Fig. 4(a), the phonon spectra along the $[001]$ direction exhibit a clear splitting within the optical branches at 6 K. A constant- q cut at the zone center shows a pronounced splitting of approximately 1 meV, corresponding to $\sim 20\%$ of the phonon energy [Fig. 4(b)]. At 100 K, this splitting vanishes, and the phonon modes recover their original profiles [Fig. 4(c)]. In contrast, no appreciable splitting is observed in FMO [Figs. 4(d)-4(f)], confirming that this effect is closely tied

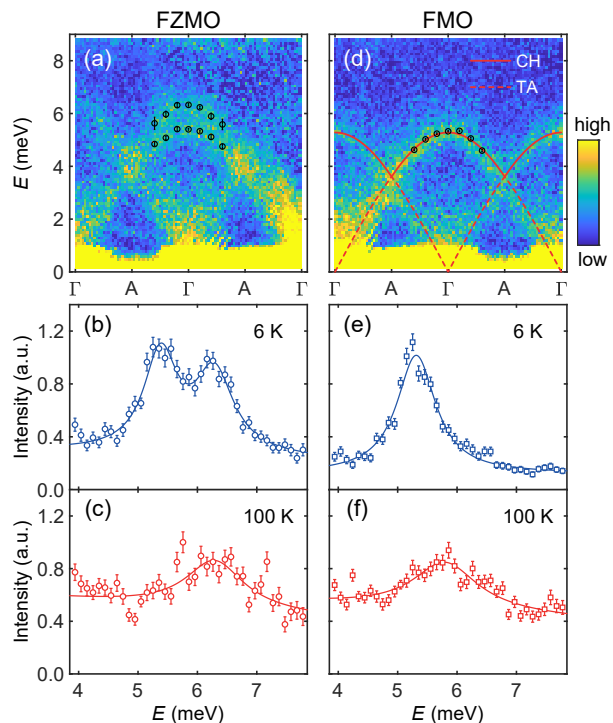


FIG. 4. (a) Phonon spectra of FZMO at 6 K along [001], integrated over equivalent Brillouin zones. Black circles mark peak positions from Lorentzian fits to various constant- q cuts. (b), (c) Constant- q cuts at zone center for 6 K and 100 K. (d)-(f) Corresponding data for FMO. Dashed and solid lines denote transverse acoustic (TA) and chiral optical phonon (CH) modes, respectively.

to the ferrimagnetic order in FZMO.

It is worth noting that the split phonon modes along the [001] direction correspond to truly chiral phonons with nonzero helicity, allowed by the discrete threefold rotational symmetry of the crystal⁵⁻⁹. In both the anti-ferromagnetic and paramagnetic phases [Figs. 4(c)-4(f)], these excitations arise from the doubly degenerate E_2 modes, primarily involving in-plane motion of Fe1 ions³⁵. Upon entering the ferrimagnetic phase [Figs. 4(a) and 4(b)], time-reversal symmetry breaking lifts this degeneracy, yielding two chiral phonon branches with opposite helicities. The splitting appears with the onset of ferrimagnetic order⁵⁹. Our zone-center constant- q cuts under magnetic field reveal opposite field dependences for the split doublet, consistent with polarization-resolved magneto-Raman measurements⁵⁹, providing additional evidence for their chiral nature (Note 5 in SM⁴³). This mechanism contrasts with earlier reports in which phonon splittings originated from inversion symmetry breaking^{4-7,30,31,38}. Moreover, the observed splitting and population imbalance between phonons of opposite chirality are consistent with the enhanced phonon thermal Hall conductivity in the ferrimagnetic phase of $\text{Fe}_{2-x}\text{Zn}_x\text{Mo}_3\text{O}_8$ ⁴¹.

A similar magnetic-order-induced splitting of chiral

phonons has been reported in the ferromagnetic Weyl semimetal $\text{Co}_3\text{Sn}_2\text{S}_2$ ^{36,37}. However, there the chiral phonons primarily originate from nonmagnetic S atoms^{36,37}, and the large energy separation between phonons and magnons renders magnon-phonon coupling negligible. In contrast, FZMO hosts strong magnon-phonon coupling, producing distinct spectral signatures in the chiral phonon branches (Fig. 3). Recently, the concept of axial phonons has been introduced as a broad class of phonons that carry angular momentum and an associated magnetic moment, while chiral phonons form a symmetry-defined subset that additionally breaks improper rotational symmetry⁶⁰. This framework naturally accounts for (i) the absence of splitting and the vanishing chiral term for the degenerate optical phonons in FMO, and (ii) the transverse acoustic phonons in both compounds (Fig. 4), which also exhibit magnetic signatures arising from axial phonon magnetic moments without requiring the symmetry constraints of true chirality.

We note that a recent theoretical study proposed that INS can distinguish chiral from linear phonons via angle-resolved measurements and by tracking phonon splitting under applied magnetic fields⁶¹. This approach considers the distinct contributions of rotational atomic motion to the nuclear dynamic structure factor. However, the magnetic scattering of chiral phonons arising from phonon magnetic moments remains largely unexplored. Polarized INS may thus provide a promising route to directly resolve phonon chirality in momentum space. Unlike magnons, whose chirality arises from the circular precession of ordered magnetic moments^{62,63}, phonon chirality originates from circular ionic motion producing effective magnetic moments. Polarized neutrons probe these phonon magnetic moments rather than the atomic rotation itself, making the detection of phonon chirality distinct from that of magnons. Developing the corresponding theoretical framework and experimental implementation represents an important direction for future research.

In summary, we present the first complete mapping of truly chiral phonon dispersions across the Brillouin zone and reveal their magnetic signature in ferrimagnetic FZMO. Below T_C , we observe enhanced magnetic scattering, out-of-plane intensity modulation, intrinsic mode splitting, and field-induced Zeeman shifts, all consistent with chiral phonons carrying substantial magnetic moments. These findings establish a direct link between magnetic order, magnon excitations, and chiral phonons in systems with strong magnon-phonon coupling, and demonstrate that neutron scattering provides a powerful, momentum-resolved probe of chiral phonons via their inherent phonon magnetic moments.

Acknowledgments—We thank Yuan Wan, Fangliang Wu, Qi Zhang and Zhao-Long Gu for stimulating discussions. The work was supported by the National Natural Science Foundation of China (Grant No. 12225407), the National Key Projects

for Research and Development of China (Grants No. 2021YFA1400400 and No. 2024YFA1409200), the National Natural Science Foundation of China (Grants No. 12434005, No. 12404173, and No. 12204160), the Natural Science Foundation of Jiangsu Province (Grants No. BK20233001, No. BK20241251, and No. BK20241250), the Natural Science Foundation of the Higher Education Institutions of Jiangsu Province (Grant No. 23KJB140012), the China Postdoctoral Science Foundation (Grants No. BX20240161 and No. 2024M751367), the Jiangsu Funding Program for Excellent Postdoctoral Talent (Grant No. 2024ZB021), the Xiaomi Young Scholars - Technology Innovation

Award, and the Fundamental Research Funds for the Central Universities (Grants No. KG202501 and No. 14380251). Part of this work is based on experiments performed at the Swiss spallation neutron source SINQ, Paul Scherrer Institute, Villigen, Switzerland. This work is also supported by J-PARC (Proposal No. 2020B0002) and ISIS (Proposal No. 2410072, DOI: 10.5286/ISIS.E.RB2410072).

Data availability—The data are not publicly available. The data are available from the authors upon reasonable request.

* These authors contributed equally to this work.; songbao@nju.edu.cn

† These authors contributed equally to this work.

‡ jwen@nju.edu.cn

¹ Lifa Zhang and Qian Niu, “Angular Momentum of Phonons and the Einstein–de Haas Effect,” *Phys. Rev. Lett.* **112**, 085503 (2014).

² Lifa Zhang and Qian Niu, “Chiral Phonons at High-Symmetry Points in Monolayer Hexagonal Lattices,” *Phys. Rev. Lett.* **115**, 115502 (2015).

³ Hao Chen, Wei Zhang, Qian Niu, and Lifa Zhang, “Chiral phonons in two-dimensional materials,” *2D Mater.* **6**, 012002 (2018).

⁴ Hanyu Zhu, Jun Yi, Ming-Yang Li, Jun Xiao, Lifa Zhang, Chih-Wen Yang, Robert A. Kaindl, Lain-Jong Li, Yuan Wang, and Xiang Zhang, “Observation of chiral phonons,” *Science* **359**, 579–582 (2018).

⁵ Kyosuke Ishito, Huiling Mao, Yusuke Kousaka, Yoshihiko Togawa, Satoshi Iwasaki, Tiantian Zhang, Shuichi Murakami, Jun-ichiro Kishine, and Takuya Satoh, “Truly chiral phonons in α -HgS,” *Nat. Phys.* **19**, 35–39 (2023).

⁶ Hiroki Ueda, Mirian García-Fernández, Stefano Agrestini, Carl P. Romao, Jeroen van den Brink, Nicola A. Spaldin, Ke-Jin Zhou, and Urs Staub, “Chiral phonons in quartz probed by X-rays,” *Nature* **618**, 946–950 (2023).

⁷ Tiantian Zhang, Zhiheng Huang, Zitian Pan, Luoju Du, Guangyu Zhang, and Shuichi Murakami, “Weyl Phonons in Chiral Crystals,” *Nano Lett.* **23**, 7561–7567 (2023).

⁸ Lun-Hui Hu, Jiabin Yu, Ion Garate, and Chao-Xing Liu, “Phonon Helicity Induced by Electronic Berry Curvature in Dirac Materials,” *Phys. Rev. Lett.* **127**, 125901 (2021).

⁹ Shuai Zhang, Zhiheng Huang, Muchen Du, Tianping Ying, Luoju Du, and Tiantian Zhang, “The chirality of phonons: Definitions, symmetry constraints, and experimental observation,” (2025), arXiv:2503.22794 [cond-mat.mtrl-sci].

¹⁰ C. Dornes, Y. Acremann, M. Savoini, M. Kubli, M. J. Neugebauer, E. Abreu, L. Huber, G. Lantz, C. A. F. Vaz, H. Lemke, E. M. Bothschafter, M. Porer, V. Esposito, L. Rettig, M. Buzzi, A. Alberca, Y. W. Windsor, P. Beaud, U. Staub, Diling Zhu, Sanghoon Song, J. M. Glowina, and S. L. Johnson, “The ultrafast Einstein–de Haas effect,” *Nature* **565**, 209–212 (2019).

¹¹ H. Zhang, N. Peshcherenko, Fazhi Yang, T. Z. Ward, P. Raghuvanshi, L. Lindsay, Claudia Felser, Yang Zhang,

J.-Q. Yan, and H. Miao, “Measurement of phonon angular momentum,” *Nat. Phys.* **21**, 1387–1391 (2025).

¹² T. F. Nova, A. Cartella, A. Cantaluppi, M. Först, D. Bossini, R. V. Mikhaylovskiy, A. V. Kimel, R. Merlin, and A. Cavalleri, “An effective magnetic field from optically driven phonons,” *Nat. Phys.* **13**, 132–136 (2017).

¹³ Jiaming Luo, Tong Lin, Junjie Zhang, Xiaotong Chen, Elizabeth R. Blackert, Rui Xu, Boris I. Yakobson, and Hanyu Zhu, “Large effective magnetic fields from chiral phonons in rare-earth halides,” *Science* **382**, 698–702 (2023).

¹⁴ M. Basini, M. Pancaldi, B. Wehinger, M. Udina, V. Unikandanunni, T. Tadano, M. C. Hoffmann, A. V. Balatsky, and S. Bonetti, “Terahertz electric-field-driven dynamical multiferroicity in SrTiO₃,” *Nature* **628**, 534–539 (2024).

¹⁵ C. S. Davies, F. G. N. Fennema, A. Tsukamoto, I. Razdolski, A. V. Kimel, and A. Kirilyuk, “Phononic switching of magnetization by the ultrafast Barnett effect,” *Nature* **628**, 540–544 (2024).

¹⁶ Dominik M. Juraschek, Michael Fechner, Alexander V. Balatsky, and Nicola A. Spaldin, “Dynamical multiferroicity,” *Phys. Rev. Mater.* **1**, 014401 (2017).

¹⁷ Dominik M. Juraschek and Nicola A. Spaldin, “Orbital magnetic moments of phonons,” *Phys. Rev. Mater.* **3**, 064405 (2019).

¹⁸ Asier Zabalo, Cyrus E. Dreyer, and Massimiliano Stengel, “Rotational g factors and Lorentz forces of molecules and solids from density functional perturbation theory,” *Phys. Rev. B* **105**, 094305 (2022).

¹⁹ C. Strohm, G. L. J. A. Rikken, and P. Wyder, “Phenomenological Evidence for the Phonon Hall Effect,” *Phys. Rev. Lett.* **95**, 155901 (2005).

²⁰ L. Sheng, D. N. Sheng, and C. S. Ting, “Theory of the Phonon Hall Effect in Paramagnetic Dielectrics,” *Phys. Rev. Lett.* **96**, 155901 (2006).

²¹ Lifa Zhang, Jie Ren, Jian-Sheng Wang, and Baowen Li, “Topological Nature of the Phonon Hall Effect,” *Phys. Rev. Lett.* **105**, 225901 (2010).

²² G. Grissonnanche, S. Thériault, A. Gourgout, M.-E. Boulanger, E. Lefrançois, A. Ataei, F. Laliberté, M. Dion, J.-S. Zhou, S. Pyon, T. Takayama, H. Takagi, N. Doiron-Leyraud, and L. Taillefer, “Chiral phonons in the pseudogap phase of cuprates,” *Nat. Phys.* **16**, 1108–1111 (2020).

²³ Dominik M. Juraschek, Tomáš Neuman, and Prineha

- Narang, “Giant effective magnetic fields from optically driven chiral phonons in $4f$ paramagnets,” *Phys. Rev. Res.* **4**, 013129 (2022).
- ²⁴ Yafei Ren, Cong Xiao, Daniyar Saparov, and Qian Niu, “Phonon magnetic moment from electronic topological magnetization,” *Phys. Rev. Lett.* **127**, 186403 (2021).
- ²⁵ Swati Chaudhary, Dominik M. Juraschek, Martin Rodriguez-Vega, and Gregory A. Fiete, “Giant effective magnetic moments of chiral phonons from orbit-lattice coupling,” *Phys. Rev. B* **110**, 094401 (2024).
- ²⁶ Qian Wang, Meng-Qiu Long, and Yun-Peng Wang, “Magnetic moments of chiral phonons induced by coupling with magnons,” *Phys. Rev. B* **110**, 024423 (2024).
- ²⁷ Bowen Ma, Z. D. Wang, and Gang v. Chen, “Chiral Phonons Induced from Spin Dynamics via Magnetoelastic Anisotropy,” *Phys. Rev. Lett.* **133**, 246604 (2024).
- ²⁸ Shuai Zhang, Kaifa Luo, and Tiantian Zhang, “Understanding chiral charge-density wave by frozen chiral phonon,” *npj Comput. Mater.* **10**, 264 (2024).
- ²⁹ Bing Cheng, T. Schumann, Youcheng Wang, X. Zhang, D. Barbalas, S. Stemmer, and N. P. Armitage, “A Large Effective Phonon Magnetic Moment in a Dirac Semimetal,” *Nano Lett.* **20**, 5991–5996 (2020).
- ³⁰ Andrey Baydin, Felix G. G. Hernandez, Martin Rodriguez-Vega, Anderson K. Okazaki, Fuyang Tay, G. Timothy Noe, Ikufumi Katayama, Jun Takeda, Hiroyuki Nojiri, Paulo H. O. Rappl, Eduardo Abramof, Gregory A. Fiete, and Junichiro Kono, “Magnetic Control of Soft Chiral Phonons in PbTe,” *Phys. Rev. Lett.* **128**, 075901 (2022).
- ³¹ Felix G. G. Hernandez, Andrey Baydin, Swati Chaudhary, Fuyang Tay, Ikufumi Katayama, Jun Takeda, Hiroyuki Nojiri, Anderson K. Okazaki, Paulo H. O. Rappl, Eduardo Abramof, Martin Rodriguez-Vega, Gregory A. Fiete, and Junichiro Kono, “Observation of interplay between phonon chirality and electronic band topology,” *Sci. Adv.* **9**, eadj4074 (2023).
- ³² Jun Cui, Emil Viñas Boström, Mykhaylo Ozerov, Fangliang Wu, Qianni Jiang, Jiun-Haw Chu, Changcun Li, Fucan Liu, Xiaodong Xu, Angel Rubio, and Qi Zhang, “Chirality selective magnon-phonon hybridization and magnon-induced chiral phonons in a layered zigzag antiferromagnet,” *Nat. Commun.* **14**, 3396 (2023).
- ³³ David Lujan, Jeongheon Choe, Swati Chaudhary, Gaihua Ye, Cynthia Nnokwe, Martin Rodriguez-Vega, Jiaming He, Frank Y. Gao, T. Nathan Nunley, Edoardo Baldini, Jianshi Zhou, Gregory A. Fiete, Rui He, and Xiaoqin Li, “Spin-orbit exciton-induced phonon chirality in a quantum magnet,” *Proc. Natl. Acad. Sci. U.S.A* **121**, e2304360121 (2024).
- ³⁴ Song Bao, Zhao-Long Gu, Yanyan Shangguan, Zhentao Huang, Junbo Liao, Xiaoxue Zhao, Bo Zhang, Zhao-Yang Dong, Wei Wang, Ryoichi Kajimoto, Mitsutaka Nakamura, Tom Fennell, Shun-Li Yu, Jian-Xin Li, and Jinsheng Wen, “Direct observation of topological magnon polarons in a multiferroic material,” *Nat. Commun.* **14**, 6093 (2023).
- ³⁵ Fangliang Wu, Song Bao, Jing Zhou, Yunlong Wang, Jian Sun, Jinsheng Wen, Yuan Wan, and Qi Zhang, “Fluctuation-enhanced phonon magnetic moments in a polar antiferromagnet,” *Nat. Phys.* **19**, 1868–1875 (2023).
- ³⁶ Mengqian Che, Jinxuan Liang, Yunpeng Cui, Hao Li, Bingru Lu, Wenbo Sang, Xiang Li, Xuebin Dong, Le Zhao, Shuai Zhang, Tao Sun, Wanjun Jiang, Enke Liu, Feng Jin, Tiantian Zhang, and Luyi Yang, “Magnetic Order Induced Chiral Phonons in a Ferromagnetic Weyl Semimetal,” *Phys. Rev. Lett.* **134**, 196906 (2025).
- ³⁷ R. Yang, Y.-Y. Zhu, M. Steigleder, Y.-C. Liu, C.-C. Liu, X.-G. Qiu, Tiantian Zhang, and M. Dressel, “Inherent Circular Dichroism of Phonons in Magnetic Weyl Semimetal $\text{Co}_3\text{Sn}_2\text{S}_2$,” *Phys. Rev. Lett.* **134**, 196905 (2025).
- ³⁸ Hiroki Ueda, Abhishek Nag, Carl P. Romao, Mirian García-Fernández, Ke-Jin Zhou, and Urs Staub, “Chiral phonons in polar LiNbO_3 ,” (2025), arXiv:2504.03330 [cond-mat.str-el].
- ³⁹ T. Kurumaji, S. Ishiwata, and Y. Tokura, “Doping-Tunable Ferrimagnetic Phase with Large Linear Magnetoelectric Effect in a Polar Magnet $\text{Fe}_2\text{Mo}_3\text{O}_8$,” *Phys. Rev. X* **5**, 031034 (2015).
- ⁴⁰ Yazhong Wang, Gheorghe L. Pascut, Bin Gao, Trevor A. Tyson, Kristjan Haule, Valery Kiryukhin, and Sang-Wook Cheong, “Unveiling hidden ferrimagnetism and giant magnetoelectricity in polar magnet $\text{Fe}_2\text{Mo}_3\text{O}_8$,” *Sci. Rep.* **5**, 12268 (2015).
- ⁴¹ T. Ideue, T. Kurumaji, S. Ishiwata, and Y. Tokura, “Giant thermal Hall effect in multiferroics,” *Nat. Mater.* **16**, 797 (2017).
- ⁴² Yuting Chang, Yakui Weng, Yunlong Xie, Bin You, Junfeng Wang, Liang Li, Jun-Ming Liu, Shuai Dong, and Chengliang Lu, “Colossal Linear Magnetoelectricity in Polar Magnet $\text{Fe}_2\text{Mo}_3\text{O}_8$,” *Phys. Rev. Lett.* **131**, 136701 (2023).
- ⁴³ See Supplemental Material at URL for experimental details, calculations and additional discussions, which includes Refs. [44-54].
- ⁴⁴ Pierre Strobel and Yvon Le Page, “Growth and morphology of single crystals of hexagonal molybdates(IV) $\text{M}_2\text{Mo}_3\text{O}_8$ ($\text{M} = \text{Mn}, \text{Fe}, \text{Co}, \text{Ni}$),” *J. Cryst. Growth* **61**, 329–338 (1983).
- ⁴⁵ P. Strobel, Y. Le Page, and S.P. McAlister, “Growth and physical properties of single crystals of $\text{Fe}_2^{\text{II}}\text{Mo}_3^{\text{IV}}\text{O}_8$,” *J. Solid State Chem.* **42**, 242–250 (1982).
- ⁴⁶ Ryoichi Kajimoto, Mitsutaka Nakamura, Yasuhiro Inamura, Fumio Mizuno, Kenji Nakajima, Seiko Ohira-Kawamura, Tetsuya Yokoo, Takeshi Nakatani, Ryuji Maruyama, Kazuhiko Soyama, Kaoru Shibata, Kentaro Suzuya, Setsuo Sato, Kazuya Aizawa, Masatoshi Arai, Shuichi Wakimoto, Motoyuki Ishikado, Shinichi Shamoto, Masaki Fujita, Haruhiro Hiraka, Kenji Ohoyama, Kazuyoshi Yamada, and Chul-Ho Lee, “The Fermi Chopper Spectrometer 4SEASONS at J-PARC,” *J. Phys. Soc. Jpn.* **80**, SB025 (2011).
- ⁴⁷ U. Stuhr, B. Roessli, S. Gvasaliya, H.M. Rønnow, U. Filges, D. Graf, A. Bollhalder, D. Hohl, R. Bürge, M. Schild, L. Holitzner, Kaegi C., P. Keller, and T. Mühlebach, “The thermal triple-axis-spectrometer EIGER at the continuous spallation source SINQ,” *Nucl. Instrum. Methods Phys. Res., Sect. A* **853**, 16–19 (2017).
- ⁴⁸ Mitsutaka Nakamura, Ryoichi Kajimoto, Yasuhiro Inamura, Fumio Mizuno, Masaki Fujita, Tetsuya Yokoo, and Masatoshi Arai, “First demonstration of novel method for inelastic neutron scattering measurement utilizing multiple incident energies,” *J. Phys. Soc. Jpn.* **78**, 093002 (2009).
- ⁴⁹ Yasuhiro Inamura, Takeshi Nakatani, Jiro Suzuki, and Toshiya Otomo, “Development status of software “Ut-susemi” for chopper spectrometers at MLF, J-PARC,” *J. Phys. Soc. Jpn.* **82**, SA031 (2013).
- ⁵⁰ R.A. Ewings, A. Buts, M.D. Le, J. van Duijn, I. Bustinduy, and T.G. Perring, “Horace: Software for the analysis of data from single crystal spectroscopy experiments at

- time-of-flight neutron instruments,” Nucl. Instrum. Methods Phys. Res., Sect. A **834**, 132–142 (2016).
- ⁵¹ Juan Rodríguez-Carvajal, “Recent advances in magnetic structure determination by neutron powder diffraction,” Physica B **192**, 55–69 (1993).
- ⁵² Laurent C. Chapon, Pascal Manuel, Paolo G. Radaelli, Chris Benson, Leigh Perrott, Stuart Ansell, Nigel J. Rhodes, Davide Raspino, D. Duxbury, E. Spill, and Julian Norris and, “Wish: The new powder and single crystal magnetic diffractometer on the second target station,” Neutron News **22**, 22–25 (2011).
- ⁵³ S. Toth and B. Lake, “Linear spin wave theory for single-Q incommensurate magnetic structures,” J. Phys. Condens. Matter **27**, 166002 (2015).
- ⁵⁴ G. Shirane, S. M. Shapiro, and J. M. Tranquada, *Neutron Scattering with a Triple-Axis Spectrometer: Basic Techniques* (Cambridge University Press, Cambridge, 2002).
- ⁵⁵ F. Varret, H. Czeskleba, F. Hartmann-Boutron, and P. Imbert, “Étude par effet Mössbauer de l’ion Fe^{2+} en symétrie trigonale dans les composés du type $(\text{Fe}, \text{M})_2\text{Mo}_3\text{O}_8$ ($\text{M} = \text{Mg}, \text{Zn}, \text{Mn}, \text{Co}, \text{Ni}$) et propriétés magnétiques de $(\text{Fe}, \text{Zn})_2\text{Mo}_3\text{O}_8$,” J. Phys. **33**, 549–564 (1972).
- ⁵⁶ D. Bertrand and H. Kerner-Czeskleba, “Étude structurale et magnétique de molybdates d’éléments de transition,” J. Phys. **36**, 379–390 (1975).
- ⁵⁷ Junbo Liao, Zhentao Huang, Bo Zhang, Yanyan Shang-guan, Shufan Cheng, Hao Xu, Zihang Song, Shuai Dong, Devashibhai Adrojia, Song Bao, and Jinsheng Wen, “Magnetic interactions in the polar ferrimagnet $\text{Mn}_2\text{Mo}_3\text{O}_8$ with a bipartite structure,” Phys. Rev. B **111**, 024407 (2025).
- ⁵⁸ Malcolm F Collins, *Magnetic critical scattering* (Oxford University Press, 1989).
- ⁵⁹ Fangliang Wu, Jing Zhou, Song Bao, Liangyue Li, Jinsheng Wen, Yuan Wan, and Qi Zhang, “Magnetic Switching of Phonon Angular Momentum in a Ferrimagnetic Insulator,” Phys. Rev. Lett. **134**, 236701 (2025).
- ⁶⁰ Dominik M. Juraschek, R. Matthias Geilhufe, Hanyu Zhu, Martina Basini, Peter Baum, Andrey Baydin, Swati Chaudhary, Michael Fechner, Benedetta Flebus, Gael Grissonnanche, Andrei I. Kirilyuk, Mikhail Lemeshko, Sebastian F. Maehrlein, Maxime Mignolet, Shuichi Murakami, Qian Niu, Ulrich Nowak, Carl P. Romao, Habib Rostami, Takuya Satoh, Nicola A. Spaldin, Hiroki Ueda, and Lifa Zhang, “Chiral phonons,” Nat. Phys. **21**, 1532–1540 (2025).
- ⁶¹ Tingting Wang, Jun Zhou, Qingyong Ren, and Lifa Zhang, “Inelastic neutron scattering for direct detection of chiral phonons,” (2025), arXiv:2507.20168 [cond-mat.mtrl-sci].
- ⁶² Y. Nambu, J. Barker, Y. Okino, T. Kikkawa, Y. Shiomi, M. Enderle, T. Weber, B. Winn, M. Graves-Brook, J. M. Tranquada, T. Ziman, M. Fujita, G. E. W. Bauer, E. Saitoh, and K. Kakurai, “Observation of Magnon Polarization,” Phys. Rev. Lett. **125**, 027201 (2020).
- ⁶³ S. Holbein, P. Steffens, S. Biesenkamp, J. Ollivier, A. C. Komarek, M. Baum, and M. Braden, “Spin-wave dispersion and magnon chirality in multiferroic TbMnO_3 ,” Phys. Rev. B **108**, 104404 (2023).
- .